



HAL
open science

Structural pattern of the Saïss basin and Tabular Middle Atlas in northern Morocco: hydrological implications

Olivier Dauteuil, Frédérique Moreau, Khaoula Qarqori

► To cite this version:

Olivier Dauteuil, Frédérique Moreau, Khaoula Qarqori. Structural pattern of the Saïss basin and Tabular Middle Atlas in northern Morocco: hydrological implications. *Journal of African Earth Sciences*, 2016, 119, pp.150-159. 10.1016/j.jafrearsci.2016.04.001 . insu-01300836

HAL Id: insu-01300836

<https://insu.hal.science/insu-01300836v1>

Submitted on 11 Apr 2016

HAL is a multi-disciplinary open access archive for the deposit and dissemination of scientific research documents, whether they are published or not. The documents may come from teaching and research institutions in France or abroad, or from public or private research centers.

L'archive ouverte pluridisciplinaire **HAL**, est destinée au dépôt et à la diffusion de documents scientifiques de niveau recherche, publiés ou non, émanant des établissements d'enseignement et de recherche français ou étrangers, des laboratoires publics ou privés.

Accepted Manuscript

Structural pattern of the Saïss basin and Tabular Middle Atlas in northern Morocco: hydrological implications

O. Dauteuil, F. Moreau, K. Qarqori



PII: S1464-343X(16)30108-X

DOI: [10.1016/j.jafrearsci.2016.04.001](https://doi.org/10.1016/j.jafrearsci.2016.04.001)

Reference: AES 2537

To appear in: *Journal of African Earth Sciences*

Received Date: 27 July 2015

Revised Date: 31 March 2016

Accepted Date: 1 April 2016

Please cite this article as: Dauteuil, O., Moreau, F., Qarqori, K., Structural pattern of the Saïss basin and Tabular Middle Atlas in northern Morocco: hydrological implications, *Journal of African Earth Sciences* (2016), doi: 10.1016/j.jafrearsci.2016.04.001.

This is a PDF file of an unedited manuscript that has been accepted for publication. As a service to our customers we are providing this early version of the manuscript. The manuscript will undergo copyediting, typesetting, and review of the resulting proof before it is published in its final form. Please note that during the production process errors may be discovered which could affect the content, and all legal disclaimers that apply to the journal pertain.

Structural pattern of the Saïss basin and Tabular Middle Atlas in northern Morocco: hydrological implications

O. Dauteuil¹, F. Moreau¹, K. Qarqori²

1) UMR-CNRS 6118 Géosciences Rennes, University of Rennes 1, 35042 Rennes cedex, France

2) Earth Sciences Department, Faculty of Sciences, Moulay Ismail University, 11201 Zitoune 50000, Meknes, Morocco

Abstract

The plain of Saïss is a fertile area of great agricultural production with major economic interests. Therefore, the improved knowledge about the water supply is imperative within a context of recurrent droughts and overexploitation of the groundwater. This plain is located in the Meknes-Fes basin and between two deformed domains: the Rif and Middle Atlas. The aquifers are fed by water coming from the Tabular Middle Atlas, for which the pathways are poorly constrained. This study provides new data to determine the water pathways based on a structural map produced from a novel analysis of SPOT images and a digital elevation model. This structural map reveals two fracture sets trending NE-SW and NW-SE. The first set is well known and corresponds to a main trend that controlled the tectonic and stratigraphic evolution of the study area. On the other hand, the NW-SE set was poorly described until now: it is both diffuse and widespread on the Tabular Middle Atlas. A comparison between the regional water flow trend, drainage pattern and structural map shows that the NW-SE fractures control the water flow from the Tabular Middle Atlas to the Saïss plain. A hydrological model is discussed where the water flow is confined onto Liassic carbonates and driven by NW-SE fractures. This study explains how a detailed structural mapping shows hydrology constraints.

Keywords: structural map, SPOT images, DEM, water circulation

1- INTRODUCTION

The Atlas chains developed from the inversion of the Jurassic rift or transtensional basins as a consequence of continental convergence between Africa and Europe during the Cenozoic. The mountain ranges are associated with high seismic activity revealing intense deformation and defining several domains with their

own history and structures (Chalouan et al., 2014). These domains are separated into less-deformed intraorogenic basins (Bargach et al., 2004; Barbero et al., 2011) (Fig. 1). The Saïss plain, associated with the Meknes-Fes basin, is one of these intraorogenic basins that separates the Rif orogen from the Middle Atlas. Terrigenous sediments, with ages ranging from the Miocene to the Pleistocene, fill this basin, which was isolated during the Miocene. The southern and northern limits correspond to thrusts that were active during the Late Miocene (Piqué et al., 2002; Frizon de Lamotte et al., 2011), and the Alpine convergence is usually assumed to have only slightly affected the basin. This unusual behaviour should be investigated to understand The regional structural analysis provided by SPOT images and digital elevation model (DEM) can be used to complete the existing data set.

The Meknes-Fes basin is a wide plain of major economic interest because of intense agriculture and the location of great cultural and touristic sites in the imperial cities of Fes and Meknes. All these human activities require large water resources that come from two aquifers: one that is deep in the Liassic units and a second shallow one in the Plio-Pleistocene deposits. The poor remediation of water rejected into the rivers (Perrin et al., 2014) imposes the use of water in the deep aquifer. The Tabular Middle Atlas, with a higher topography and higher rainfall, mainly supplies the two aquifers. Water flow connections between these two domains remain poorly constrained and must be investigated to improve the management of water resources in this region. The water pathways are controlled by several parameters including the rock porosity, lithology, fracture pattern and structure layering. However the investigation to determine these pathways is complex and requires combined approaches. Thus, we propose to use surface structural mapping based on by SPOT images and DEM interpretation, combined with drainage pattern and hydrological information, to determine the potential water pathways.

2- GEOLOGICAL AND HYDROLOGICAL SETTINGS

2.1- Geological framework

The Middle Atlas and Rif mountains represent two major structural domains in northern Morocco that are separated by the Fes-Meknes basin (Fig. 1). The Middle Atlas shows two different geomorphic areas (Barcos et al., 2014): a northwest domain with tabular relief (the Tabular Middle Atlas or TMA), and a northeast-southwest domain with a mountainous relief linked to the High Atlas. The TMA represents a key area for the water supply of the Saïss plain associated with the Fes-Meknes basin. The TMA is a large karstic reservoir from which water flows out to the plain. However, the water circulation paths are not precisely constrained, and this is one of the aims of this study.

The TMA has a roughly flat topography at an elevation of 1100 m on the western side while the eastern side is higher (1400 m) and more incised. NE-SW linear and long valleys and NW-SE short valleys shaped the topography (Fig. 2). The western flat part is sparsely covered by vegetation while the eastern mountainous part is largely covered by vegetation, mainly forests. The southern border of the TMA corresponds to erosion scarp that forms a window on the basement of the TMA. To the north of the TMA, the Saïss basin forms a plain with a total surface area of 2,100 km² and northward regional tilting: 850 m in the south and 525 m in the north, i.e. an approximate regional slope of 1%. To the NE of the plain, the Fes sub-basin has a flat morphology that is 130 m lower than the western sub-basin. This plain is deeply incised on the borders of the western and northern

71 sides, while there are very few rivers in the middle and southern parts. The main streams trend NE-SW and E-
72 W (Fig. 2). The Saïss plain and the TMA have the same geological evolution until the Cenozoic. Triassic
73 evaporites unconformably cover the Palaeozoic basement that was deformed during the Hercynian orogeny.
74 During the Liassic opening of the Tethysian Ocean, carbonates (limestones and dolomites) with significant
75 thicknesses were deposited. In the study area, this extension trends NW-SE, which generated NE-SW blocs
76 controlling the deposit centres. Then, a large depositional gap occurred until the Neogene and the evolution of
77 the TMA and Saïss basin diverged (Ennadifi, 1975; Arboleya et al., 2004; Amraoui, 2005; Qarqori et al., 2012).
78 During the Late Miocene, the Fes-Meknes basin in the north became a deep marine trough trending NE-SW and
79 filled with a thick sequence of shales with turbidites (Charroud et al., 2007; Bachiri Taoufiq et al., 2008). Then,
80 a main environmental change occurred during the Plio-Quaternary generating the depositional context, evolving
81 from lacustrine to fluvial with lacustrine limestone, conglomerate and sandstone deposits. This change resulted
82 in a general uplift of the whole study area. Also, the deposit of a significant amount of travertine on the northern
83 edge of the TMA should be noted (Chamayou et al., 1975). Since the late Miocene, the TMA became a horst
84 that was emerged until now. The Liassic carbonates were largely weathered, generating a large karstic plateau
85 with the emergences of springs at the junction with the Saïss basin. During the Pleistocene, the plateau was
86 locally covered by alkaline basalt lava flows coming from the Outgui volcano and flowing to the Saïss plain
87 into the pre-existing valley. A recent GPS study (Chalouan et al., 2014) reveals that the contact between the two
88 domains is affected by a slow divergence associated with normal faults with a dextral slip component, trending
89 NE-SW.

90 The TMA displays two fault sets: one trending NE-SW corresponding to the main faulted zones that are
91 well known in the Rif domain and in the Middle Atlas (Morel, 1989, Aït Brahim and Chotin, 1989; Aït Brahim
92 et al., 2002; Frizon de Lamotte et al., 2009; Vergés and Fernandez, 2012) and a second one oriented NW-SE that
93 has been less described (Amraoui, 2005). This latter trend is locally described in the Middle Atlas, Rif ranges
94 (Aït Brahim et al., 2002) and Alboran basin (Vergés and Fernandez, 2012). The main NE-SW faulted corridors
95 located on the TMA did not affect these recent basaltic flows. The structural framework of the Saïss basin is
96 poorly defined because of the vegetation cover. Morel (1989), Aït Brahim and Chotin (1989), Amraoui (2005),
97 Aït Brahim et al. (2002), and Frizon de Lamotte et al. (2009) described a set of NE-SW features for which the
98 locations and types have been debated: normal faults, strike-slip faults or flexures.

99 2.2- Hydrological context

100 The water supply for human activities in the Saïss plain comes from three locations: a shallow aquifer
101 located in the Plio-Pleistocene sediments, a deep aquifer located within the Liassic dolomites and limestone, and
102 springs located on the boundary between the TMA and the plain. Although rainfall mainly feeds the shallow
103 aquifer, the deep aquifer is filled both by infiltration coming from the surface water and by deep circulations of
104 water coming from the TMA (Amraoui, 2005; Belhassan, 2011). The recharge of aquifer located inside the Saïss
105 basin is largely controlled by precipitation occurring in the TMA (Amraoui, 2005; Belhassan, 2011). The high
106 elevations of the TMA favour rainfall that penetrates inside the Liassic dolomite karst. The rainfall can reach
107 1000 mm/yr close to Ifrane, which is twice as high as in the plain (550 mm at Meknes, for instance). In the Atlas
108 plateau, the surface run-off is restricted because of the presence of fractures and dissolution sinks forming the
109 karst system at depth. The water primarily flows northward and comes out of the base of the TMA through

110 several springs mainly located between the area of Ribaa and Bittit (Bentayeb and Leclerc 1977). Essahlaoui et
111 al. (2001) and Qarqori et al. (2012) used a geo-electrical tomography survey to explore the structural pattern at
112 the junction between the TMS and the plain, close to the Bittit spring (Fig. 2). These geophysical surveys
113 established a structural framework for the deep aquifer located in the Liassic formation. Qarqori et al. (2012)
114 pointed out northward to north-westward water circulations in the Bittit spring through sub-vertical fractures and
115 horizontal joints. However the fracture pattern driving the water flow has not been described in classical
116 structural work. We propose to carry out a complete structural investigation to better constrain the water
117 circulation filling the aquifers.

118

119 **3- METHODOLOGY AND DATA**

120 The first step of this study is to create the most comprehensive map possible of the structures
121 affecting the area. Then the map is compared to local hydrogeological data to propose which deep and connected
122 features are potential water drains. We focus more specifically on regional features, which connect the TMA to
123 the Saïss plain. In the studied region, remote data such as satellite images or DEM provide widespread coverage
124 that can be used to integrate the whole aquifer system from the filling area to the aquifer. The proposed
125 methodology is based on a coupling between the analysis of the satellite imagery (SPOT images) and DEM data
126 in order to extract pertinent lineations that may be related to the surface geology and not to human activities. The
127 DEM was processed using the LandSerf software (version 2.3.1) developed by J. Wood. This kind of structural
128 map is classically used in addition to field observations to infer the deformation history of a region. We improve
129 the use of this map by comparing it to pre-existing hydrological work. Different processing techniques for the
130 satellite images that are particularly adapted to extract hydrogeological information are proposed. These maps
131 and the hydrological data were integrated into a GIS (QuantumGIS) and were interpreted by coupling the
132 different images produced.

133

134 **3.1- Satellite images**

135 Satellite images are powerful data to map geological objects over large areas. However, the vegetation
136 masks the structural pattern in several places. In order to cover the entire Saïss plain region, seven SPOT images
137 (Figs. 3 and 4) were used with a pixel size ranging from 2.5 m to 10 m and with different spectral modes (see the
138 more detailed technical description in Table 1 and locations in Figure 3). We restricted the image processing to
139 classical methods that can be used to extract structures: dynamic stretching, contrast enhancements (Fig. 4) and
140 edge detections. We focused on methods extracting linear objects that can be interpreted as structural features
141 (fractures, faults, schistosity and stratas). The edge extraction was done with Sobel filters composed of four
142 diagonal matrixes of 5x5 pixels corresponding to the N-S, E-W, NE-SW and NE-SW directions, respectively
143 (Fig. 5). These different calculations reveal several lineaments and features that are more visible on the TMA
144 and more discrete on the plain of Saïss. These differences can be attributed to the vegetation, the development of
145 which is largely controlled by human activities in the plain compared to the TMA, to the lithology of the
146 basement (carbonate versus terrigenous sediment, respectively) and to the deformation history, which is different
147 in the two domains. By combining the results provided by SPOT images with DEM interpretations, the
148 differences due to human activities and to vegetation can be filtered out.

149 3.2- Digital topography

150 The relief provides information about geology because it is sensitive to the structure (fault, strata
151 orientation) and to differential erosion induced by the lithological contrast. The digital topography can be
152 processed to extract structural data (Dauteuil, 1995). We used SRTM DEM with a pixel size of 30 m to analyse
153 the pattern of the topography and to extract features that will be compared to those coming from the analysis of
154 the SPOT images (Fig. 3). The plain of Saïss displays a relatively flat morphology, and consequently we used
155 geomorphic indexes to extract the structural and geological features that were subsequently correlated to the
156 features mapped from the SPOT images. To extract the structural features, we used both the usual processing
157 techniques, such as shaded images with different light directions (Fig. 6), and slope calculations (Fig. 7)
158 (Dauteuil, 1995). We analysed the average slopes at different scales by estimating the azimuth and dip of a mean
159 plane supported by points belonging to a moving window. The best-adjusted plane was calculated by a least
160 squares fitting. Two windows were calculated: a small one (2.5 x 2.5 km) for the smaller scale and a large one
161 (7.5 x 7.5 km) for the larger scale. The result of this slope analysis will be compared to the drainage pattern
162 because of the strong a priori correlation between the water flows and slope direction. Finally, the feature
163 network including the channel, isolated peaks and topographic ridges was extracted (Fig. 8) via processing with
164 the LandSerf GIS software (Fisher et al., 2004; Wood, 2013).

165 4- RESULTS

166 4.1- Interpretation of the SPOT images

167 The SPOT images show large differences in the radiometric pattern between the TMA, Palaeozoic
168 basement and plain. The Palaeozoic basement shows well-defined ridges trending at N030° with sparse
169 vegetation (shown in red in the pseudo-colour image – Fig. 4). The TMA displays various radiometric types: the
170 dark red colour corresponds to forests; the medium grey colour indicates volcanic flows and the heterogeneous
171 grey-to-red areas delineate a mixture between grass and rock. Conversely to the basement, no main organized
172 features are noticeable on the TMA, except in the NE part where wide and narrow linear valleys trend at N030°.
173 Close to the border with the plain, some narrow and short valleys are oriented approximately N300°. In the Saïss
174 plain, the radiometric pattern is very heterogeneous with several small patches of various colours (light grey,
175 dark grey, white and red) with regular shapes. This pattern is driven by human activities (crop field, roads,
176 farms, etc.). There is no main organization or linear feature, except for a tiny NW-SE-oriented trend associated
177 with farming and small rivers, especially in the north of the plain, around the town of Meknes.

178 The results of the contour detection techniques confirm and highlight the previously described structural
179 characteristics. Figure 5 provides representative zooms of two different Sobel processing operations with the
180 dominant features. The direction of the lineaments in the TMA is relatively homogeneous compared to the well-
181 shaped basement and fined-shaped plain. NNE-SSW features are well extracted on the basement in the south and
182 in the TMA, while they are scarcer in the plain. A NW-SE trend dominates the structural pattern of the plain: the
183 features are thin and close to each other. In addition, some NE-SW linear features are localized in corridors that
184 have the same trend (upper image in Fig. 5). A large number of extracted lineaments are associated with farm
185 fields. The MNT analysis must be used together with this SPOT contour image to identify the anthropogenic

186 lineaments. The combined analysis of remote images and DEM allow geological lineaments to extract. This
187 NW-SE direction is scarcely reported in field studies while it appears clearly on satellite images.

188 4.2- Topography analysis

189 The topography that is less sensitive to the vegetation may constitute powerful complementary data to
190 extract tectonic features. The shaded images (Fig. 6) and slope calculations at different scales (Figs. 7a and 7b)
191 display different relief patterns in the Palaeozoic basement, TMA and Saïss plain. Regardless of the scale, the
192 Saïss plain has the gentlest slopes with highest values organized into narrow bands trending NW-SE and WNW-
193 ESE, corresponding to permanent or semi-permanent rivers and to local anomalies on the topographic surface.
194 As expected, the rugged relief of the TMA shows the highest values coming from elevated relief relative to the
195 surrounding areas and the tectonics, seen both on the slope and in the shaded images. The slopes are mainly
196 organized into NE-SW bands, except to the NE of El Hajeb where the TMA border displays NW-SE short
197 valleys. The Palaeozoic basement clearly shows NE-SW reliefs with high slopes separated by narrow flat plains.
198 At local scales, the slopes (2.5 x 2.5km window) do not display well-organized azimuth trends: the slopes plunge
199 roughly perpendicular to the relief with a maximum toward the N to NNE. At a more regional scale (7.5 x 7.5
200 km window), the slopes gradually plunge northward in the south to westward in the plain with a maximum
201 trending NW. The Rif area shows slopes plunging NE to ENE. We compare the slope plunge to the river
202 drainage direction in Figure 7: the river streams mainly trend N-S and NW-SE. These trends are slightly
203 different by 10° from the maximum slope plunge, indicating that the regional slope partially drives the river
204 trends and that another process should be inferred as a consequence (Fig. 7).

205 The geomorphic structure network (Fig. 8) confirms the difference in morphology patterns between the
206 TMA, plain and Rif domain. The structure network is denser in the TMA and Palaeozoic basement than in the
207 Saïss plain. In the plain, ridges are almost absent near the TMA while they are well developed in the NW part
208 around the town of Meknes where they separate into channels, i.e. drains. The channels in the plain display a
209 dendritic pattern close to the TMA border and long streams in the middle of the plain. Topographic ridges are
210 absent on the southern border of the plain. This change in drainage pattern corresponds to a change in drainage
211 direction from NNW-SSE to NW-SE. These changes in the drainage pattern characteristics and the limit of the
212 topographic ridges correspond to a NE-SW trending band (Fig. 8) that separates the Saïss plain into two
213 domains: the NW part and SE part. On the border with the TMA, a lot of drains are associated with springs
214 located on the mid-slope of the relief between the two domains. In the TMA, the drainage pattern corresponds to
215 an irregular dendritic pattern with well-nested topographic ridges and channels. The channels and ridges have
216 short and wavy segments. The main and longer channels trend NE-SW.

217 **5- Interpretations**

218 5.1- Structural pattern

219 The combined interpretation of the SPOT images and topography allows us to produce a structural map
220 to establish the tectonic relationships between the TMA and plain (Fig. 9). The analysis also reveals that the
221 structural pattern of the study area is driven by two perpendicular sets of lineaments: NE-SW and NW-SE.

222 The NE-SW structures dominate the shape of the TMA: they correspond to well-known features in the
223 Atlas domain and Rif domain (Morel, 1989, Aït Brahim and Chotin, 1989; Aït Brahim et al., 2002; Frizon de
224 Lamotte et al., 2009; Vergés and Fernandez, 2012). They affect the entire area, and some corridors display more
225 fractures generating long valleys with a flat bottom. The displacements along these features cannot be
226 determined from this analysis because of the lack of well-defined markers. However, the geomorphic shape of
227 these features indicates both vertical and horizontal components in agreement with previous studies (Aït Brahim
228 et al., 2002; Arboleya et al., 2004; Bargach et al., 2004; Frizon de Lamotte et al., 2009). This work points out
229 that NE-SW features localized into restricted corridors affected the plain of Saïss (Fig. 9). These latter corridors
230 were previously described as bends by Fassi (1999) and Amaraoui (2005): the Toudal bend, Kouidiart Zouarl
231 bend, Souk Jemad El Gour bend and Boufekrane - Haj Kaddour bend. These features drive the orientation and
232 type of drainage network, and correspond to discontinuous slope breaks. This direction was active since the
233 Triassic and controlled the Triassic to middle Jurassic deposits (Piqué et al., 2002; Frizon de Lamotte, 2009) and
234 the Miocene filling of the Saïss basin (Essahlaoui et al., 2000; 2001; Amaraoui, 2005). This structural set is
235 partially imaged at depth with seismic profiles (Zizi, 2002) displaying a fault inside the Cenozoic deposits that is
236 in agreement with stratigraphic correlations from boreholes (Charroud et al., 2007). Electrical surveys
237 (Essalahoui et al., 2000) highlight a NW-SE structural trend that is well-organized at depth (4 km).

238 The NW-SE structural set was found in the whole study area with various patterns. In the TMA, it is
239 diffuse and associated with narrow V-shape valleys. In some places, these features offset NE-SW structures
240 indicating a strike-slip component. This trend is less described than the NE-SW features. Aït Brahim and Chotin
241 (1989) and Vergés and Fernandez (2012) suggest strike-slip fault zones accommodating deformation transfer.
242 The plain of Saïss is affected by tiny and diffuse NW-SE fractures. This deformation is widespread over the
243 plain and corresponds to a set of short segments compared to the NE-SW band, which has longer and localized
244 segments. The fractures of the NW-SE band control some permanent and semi-permanent rivers to the south of
245 the town of Meknes. Close to the TMA, this set is not systematically associated with drainage features. In the
246 depression of Fes, deformation appears to be less intense and less widespread. The associated features
247 correspond to changes in the slope and with small rivers. The structural set was previously poorly described
248 because it corresponds to a pattern of widespread fracturing that can be observed at the outcrop scale (Qarqori et
249 al., 2011). The geophysical surveys did not describe this in depth, probably because it corresponds to diffuse
250 features that are difficult to image with classical geophysical methods. However, an electrical survey (Essalahoui
251 et al., 2002; Essahlaoui and El Ouali, 2003) displays anomalies trending NW-SE at 100 and 1000 m in the
252 western part of the Saïss basin, fitting with this structural trend. Thus, the NW-SE features detected at the
253 surface are present at depth.

254

255 5.2- Deformation timing

256 A deformation timing can be advanced from geological arguments and from the new observations
257 coming from this study. First of all, the two sets of structures did not affect the volcanic flows dated as late
258 Quaternary or the Pleistocene sediments; however, they do affect the Pliocene deposits, revealing that they
259 occurred at the end of the Pliocene. The relative chronology between the two fracture sets can be determined

260 locally where the NW-SE fractures offset the NE-SW features. At the regional scale, the contact between the
261 TMA and the Saïss basin trends NE-SW, and it is often locally offset by NW-SE faults. Therefore, the NW-SE
262 features were generated after the NE-SW features. These faulted zones have been previously described (Aït
263 Brahim et al., 2002; Piqué et al., 2002; Arboleya et al., 2004) and seem to control, at least partially, the
264 depositional centres and deformation in these areas since the Late Triassic (Jabour et al., 2004; Frizon de
265 Lamotte et al., 2009). They were interpreted as resulting from the reactivation of the Liassic fault systems during
266 the different Mio-Pleistocene events. During the Late Miocene, this fault set played a major role in the
267 generation of horsts and grabens. The larger horst is the TMA, which was isolated from the Saïss basin by a
268 major normal fault (Aït Brahim et al., 2002). The elevated topography of the TMA was acquired at this time
269 because no marine shales were described on this plateau. Inside the basin, the normal NE-SW faults confined
270 several depositional centres with variable thicknesses. The deformation period corresponds to a NW-SE
271 stretching. During the Pliocene, they were reactivated as steep thrusts probably with a strike-slip component
272 (Bargach, et al., 2004; Charroud et al., 2007). This change in fault kinematics is consecutive to a rotation of the
273 regional stresses. This deformation is not still very active because many of the features were sealed by lava flows
274 and travertines during the Middle to Late Pleistocene.

275 The diffuse deformation generated late NW-SE features. This deformation is recent and happened
276 during a short event. It partially controlled the erosion of the TMA by generating short valleys and the new
277 setting of the rivers in the basin, especially around the town of Meknes. The deformation is associated with a
278 NE-SW stretching and is compatible with the NW-SE to N-S trends of compression described by Bargach et al.
279 (2004). The genesis of these feature sets favoured the location of a new drainage pattern, which was formed
280 during a base level fall. This change in drainage reorganization corresponds to the palaeogeographic drying of
281 the Pleistocene lake after a fast withdrawal compatible with the base level fall.

282 5.3- Hydrogeological outcomes

283 This work determined the fracturing pattern of the study area in order to propose which structure set is
284 the most efficient to drain water from the TMA to the plain. We will investigate the possible structural
285 pathways: the two fracture sets described before, and the stratigraphic layering, which corresponds to horizontal
286 or sub-horizontal drains located both in the TMA and in the Fes-Meknes basin (Fig. 1). The most significant
287 difficulty is to extrapolate 2D surface data to the 3D connected deep network. Due to the lack of geophysical
288 surveys at the regional scale, we used indirect observations.

289 The first-order field evidence of water circulation coming from the TMA is the presence of many springs
290 located at the junction between the TMA and the plain (Fig. 10), close to the unconformity between the
291 dolomitic karst and the Palaeozoic basement (Zarhloule, et al. 2001; Amraoui 2005). They are mainly gathered
292 in two places: west of El-Hajeb and west of Ain Bittit (Fig. 10). The springs around Ain Bittit are located in the
293 area where the topographic transition between the TMA and plain is smooth compared to other places. This area
294 is also characterized by recent deposits of travertine that are absent in other places on the northern border of the
295 TMA (Ennadifi, 1975). The superposition of the springs on the fracturing map reveals that they are clearly
296 located in the continuation of the NW-SE features of the TMA, and not in the continuation of the NE-SW

297 features. This result is in agreement with the interpretation of Qarqori et al. (2012), who proposed that NW-SE
298 fractures are the main water drains.

299 The TMA is mainly composed of Liassic karst affected by NE-SW fault-driven corridors and NW-SE
300 widespread features. The two features affect the Mesozoic units at depth and could be drains for the circulation
301 of water. These drains can favour both rainfall percolations at depth, because their sub-vertical dip, and lateral
302 water connectivity at depth. This work points out that the NW-SE structures drive the lateral connectivity at
303 depth and favour karst development by increasing the carbonate dissolution generating the karstic caves. Two
304 hypotheses are proposed to explain the low connectivity of the NE-SW features: 1) they either juxtapose blocks
305 with contrasted porosity, or 2) they are sealed with clay coming from the Miocene shales. Amraoui (2005) and
306 Belhassan (2011) conducted a detailed analysis of the hydrology of the deep aquifer both in the TMA and the
307 plain. Based on a large piezometer dataset, these authors built a map of the depth of the water table and deduced
308 a northward flow of the water (Fig. 10). They proposed flow lines for which the trends are perfectly compatible
309 with the water circulations along the NW-SE features both in the TMA and the plain of Saïss.

310 Figure 11 illustrates a model of water circulation from the TMA to the Neogene basin of Fes-Meknes
311 taking into account both the previously described hydrological data and the new structural pattern stemming
312 from this work. The precipitation occurring on the elevated relief of the TMA percolate into the Liassic
313 dolomites across a fracture drain. A Triassic clay layer above the unconformity with the basement confines the
314 circulation into the carbonate layers. The northward general dip of the stratigraphic layers of the TMA drives a
315 northward migration of the water confined in the carbonate layers. The northern margin of the TMA is formed
316 by a set of blocks of Mesozoic units limited by faults (Chalouan et al., 2014). These blocks collapse toward the
317 deepest parts of the basin. The vertical throw along the normal faults is low enough to not disconnect the water
318 paths to the basin. In addition to this regional pattern, the drainage is driven by NW-SE fractures that constitute a
319 widespread network both in the TMA and in the basin. The combination of the regional faults trending NE-SW
320 and the NW-SE fracture set generates a complex pattern of blocks that are more or less disconnected depending
321 on the fault throws.

322

323 **6- Conclusions**

324 This study proposes a model of structural relationships between the Saïss basin and Tabular Middle
325 Atlas. It points out the efficiency of combining an analysis using both SPOT images and DEM to propose a
326 structural map. Two fault sets were extracted: a well-known one trending NE-SW and a new one oriented NW-
327 SE, both affecting the TMA and the basin. The NE-SW structures correspond to faulted corridors in the TMA
328 and tiny flexures in the basin, initiated during a NW-SE extension occurring in the Late Miocene and
329 corresponding to reactivated Liassic faults. The NW-SE structures correspond to a diffuse and ubiquitous
330 deformation that affected the whole study area. This direction of deformation is clearly visible on satellite
331 images after processing on the slope map of the MNT, while it was somewhat identified in previous studies on
332 the region. These fracture sets control the dissolution of carbonates in the TMA forming the karst network and
333 the development of the drainage pattern in the plain. We examined the consequences of this structural pattern in
334 terms of hydrology, especially for the water connectivity between the TMA and the basin. A comparison with

335 hydrological data reveals that these NW-SE features constitute the main connectivity for the deep-water
336 circulations from the TMA to the basin. At least, we propose that water pathways are connected via diffuse
337 fracture porosity rather than by a localized drainage system. This study highlights the fact that a study combining
338 classical structural methods and hydrological data may significantly constrain the hydrology of an area.

339

340 **Acknowledgments:**

341 The work is part of the IRD program CORUS II that was funded by the Foreign Office of the French
342 government. The Spot images were acquired using the ISIS program supported by CNES, SPOT Image and
343 IGN. The cooperation program CNRS France/CNR Morocco funded the field trips. We thank the two reviewers
344 and the editor whose comments improved the initial manuscript.

345

ACCEPTED MANUSCRIPT

346

347 **Figure Captions.**

348 **Figure 1:** Location of the study area. a) Location map with the topography of northern Morocco, b) 3D view of
349 the study area using Google Earth (image data: Google, DigitalGlobe) with the main morpho-structural
350 units (red lines), c) N-S geological cross-section showing the different units.

351 **Figure 2:** Simplified geological map of the study area modified from a geological map (Ennadifi, 1975 and
352 Amraoui 2005).

353 **Figure 3:** Map of the study area with the data used in this study. The red squares identify the SPOT images with
354 the index number in the red tag. The relief map in the background is taken from the SRTM database with a
355 pixel size of 90 m.

356 **Figure 4:** Mosaic of the SPOT images used in this study. Table 1 summarizes the main characteristics.

357 **Figure 5:** Extraction of the contours based on the convolution techniques carried out using a diagonal matrix
358 (Sobel filters). To better illustrate the processing, we only display two zooms of the two Sobel processing
359 operations. Upper image: zoom of the middle part of the Saïss plain showing a NE-SW lineament
360 highlighted by a N-S diagonal matrix. Middle image: zoom of the NE-SW lineaments of the TMA
361 extracted with a NW-SE diagonal matrix.

362 **Figure 6:** Shaded images of the topography: a) light coming from the north, b) light coming from the east.

363 **Figure 7:** Distribution of the slopes at different scales. The adjusted plane was calculated in window of varying
364 sizes (grey grid): a- 2.5 x2.5 km, b-7.5x7.5 km. The red lines indicate the trend and the relative value of the
365 slope. On the left side, we plot: i) the polar diagrams of the azimuth versus the plunge of the slope and ii)
366 the rose diagrams of the slope directions (in red) and river orientations (in blue).

367 **Figure 8:** Topographic surface network. The ridges in yellow and the channels in blue were extracted from the
368 DEM with the Landserf software using a method developed by Wood (2000) and Schneider and Wood
369 (2004). This processing technique well illustrates the contrasted topography between the plain and the
370 TMA. It can be used to distinguish between several domains in the plain with different ridge and channel
371 networks.

372 **Figure 9:** Structural map of the detected features on the right with a shaded relief as the background. In the left
373 column, a half rose diagram of the fault orientation. The lower diagram in the left column displays the
374 length distribution of the features.

375 **Figure 10:** Water pathways and fractures in the study area. The contour of the water table and the theoretical
376 water flows are taken from Amraoui (2005) and Belhassan (2011). The deep water circulates toward the
377 northwest. The flow direction fits with the NW-SE features both in the TMA and in the Saïss basin. The
378 spring locations come from the geological map and from Amraoui (2005) and Belhassan (2011).

379 **Figure 11:** Schematic section of the TMA and Saïss plain showing the inferred hydrological relationships
 380 between the three aquifers: the karst of the TMA, the superficial free aquifer and the deep confined aquifer
 381 of the plain. The water circulation coming from the karst of the TMA is driven both by regional faults
 382 trending NE-SW and by a widespread fracture trending NW-SE. The two structural sets generate a complex
 383 pattern inside the basin making it difficult to implement the drilling.

384

385 **Table 1** Main characteristics of the SPOT images.

| Scene | SPOT | upper left corner | upper right corner | lower left corner | lower right corner | Image type | Pixel size | Date |
|------------------|------|----------------------------|----------------------------|----------------------------|----------------------------|------------|------------|------------|
| 0161003-2 | 5 | N34°1'49" W4°57'41" | N33°53'34" W4°19'18" 3 | N33°22'3" W4°29'7" | N33°30'16" W5°7'17" | PAN | 5 m | 2006-10-14 |
| 0161003-1 | 2 | N033°57'32" W005°42'14" | N033°51'31" W005°04'05" | N033°25'56" W005°51'31" | N033°19'57" W005°13'36" | XS | 20 m | 2007-10-21 |
| 0161003-3 | 5 | N33°58'40" W4°58'39" | N33°50'25" W4°20'17" | N33°18'53" W4°30'6" | N33°27'6" W5°8'14" | PAN | 5 m | 2006-10-14 |
| 0161003-4 | 4 | N033°51'02" W005°17'04" | N033°45'23" W004°38'24" | N033°19'22" W00525'49" | N033°13'45" W004°47'23" | XI | 20 m | 2007-02-28 |
| 0189121-1 | 4 | N034°00'46" W005°45'22" | N033°54'46" W005°07'15" | N033°29'10" W005°54'38" | N033°23'12" W005°16'45" | XI | 20 m | 2006-01-18 |
| 0157076-1 | 5 | N34° 34'13" W5° 21'30" | N34° 26'37" W4° 43'28" | N33° 55'2" W4° 52'48" | N34° 2'36" W5° 30'36" | PAN | 5 m | 2006-11-30 |
| 0157076-2 | 5 | N33° 44'34" W5° 36'17" | N33° 36'59" W4° 58'37" | N33° 5'23" W5° 7'48" | N33° 12'56" W5° 45'16" | HI | 10 m | 2006-11-30 |

386

387

- 388 References:
 389
 390 Aït Brahim, L., Chotin, P., Hinajc, S., Abdelouafia, A., El Adraouia, Nakcha, C., Dhont, D., Charroud, M.,
 391 Sossey Alaoui, F., Amrhar, M., Bouaza, A., Tabyaoui, H., Chaouni, A. 2002. Paleostress evolution in the
 392 Moroccan African margin from Triassic to Present. *Tectonophysics* 357, 187–205.
 393
 394 Amraoui, F., Razack, M., Bouchaou, L., 2004. Comportement d'une source karstique soumise à une sécheresse
 395 prolongée : la source Bittit (Maroc). *C. R. Geoscience*. 336, 1099–1109.
 396
 397 Amraoui, F. 2005. Contribution à la connaissance des aquifères karstiques : cas du Lias de la plaine de Saïss et du
 398 Causse moyen atlasique tabulaire (Maroc), Faculté des Sciences. Université Hassan II Ain Chock,
 399 Casablanca, pp. 249.
 400
 401 Arboleya, M.L., Teixell, A., Charroud, M., Julivert, M., 2004. A structural transect through the High and Middle
 402 Atlas of Morocco. *Journal of African Earth Sciences*. 39, 319–327.
 403
 404 Bachiri Taoufiq, N., Barhoun, N., Suc, J.-P., 2008. Les environnements continentaux du corridor rifain (Maroc)
 405 au Miocène supérieur d'après la palynologie. *Geodiversitas*. 30, 41-58.
 406
 407 Barbero, L., Jabaloy, A., Gómez-Ortiz, D., Pérez-Peña, J.V., Rodríguez-Peces, M.J., Tejero, R., Estupiñán, J.,
 408 Azdimousa, A., Vázquez, M., Asebriy, L., 2011. Evidence for surface uplift of the Atlas Mountains and the
 409 surrounding peripheral plateaux: Combining apatite fission-track results and geomorphic indicators in the
 410 Western Moroccan Meseta (coastal Variscan Paleozoic basement). *Tectonophysics*. 502, 90–104.
 411
 412 Barcos, L., Jabaloy, A., Azdimousa, A., Asebriy, L., Gómez-Ortiz, D., Rodríguez-Peces, M.J., Tejero, R., Pérez-
 413 Peña, J.V. 2014. Study of relief changes related to active doming in the eastern Moroccan Rif (Morocco)
 414 using geomorphological indices, *Journal of African Earth Sciences*, 100, 493-509,
 415
 416 Bargach, K., Ruano, P., Chabli, A., Galindo-Zaldivar, J., Chalouan, A., Jabaloy, A., Akil, M., Ahmamou M.,
 417 Sanz de Galdeano, C., Benmakhlouf, M., 2004. Recent Tectonic Deformations and Stresses in the Frontal
 418 Part of the Rif Cordillera and the Saïss Basin (Fes and Rabat Regions, Morocco). *Pure applied geophysics*.
 419 161, 521–540.
 420
 421 Belhassan, K., 2011. Hydro-Geological Context of Groundwater Mikkés and Different Variations of its Springs
 422 Flows (Morocco). *Research Journal of Earth Sciences*. 3, 15-26.
 423
 424 Bentayeb, A., Leclerc, C., 1977. Le Causse moyen- atlasique, in: Editions du Service Géologique du Maroc
 425 (Ed.), *Ressources en Eau du Maroc*, 37-84.
 426
 427 Chalouan, A., Gil, A.J., Galindo-Zaldívar, J., Ahmamou M., Ruano, P., de Lacy, M.C., Ruiz-Armenteros, A.M.,

- 428 Benmakhlouf, M., Riguzzi, F. 2014. Active faulting in the frontal Rif Cordillera (Fes region, Morocco):
429 Constraints from GPS data, *Journal of Geodynamics*, 77, 110-122.
- 430
- 431 Chamayou, J., Combe, M., Genetier, B., Leclerc, C., 1975. Le bassin de Meknès-Fès , in: Maroc, E.d.S.G.o.d.
432 (Ed.), *Ressources en Eau du Maroc*. 41-71.
- 433
- 434 Charroud, M., Cherai, B., Benabdelhadi, M., Falgere, C., 2007. Impact de la néotectonique Quaternaire sur la
435 dynamique sédimentaire du Saïss (Maroc) : du bassin d'avant fosse Pliocène au plateau continental
436 Quaternaire. *Quaternaire*. 18, 327-334.
- 437
- 438 Dauteuil, O., 1995. Fault pattern from Seabeam processing: the Western part of the Blanco fracture Zone (NE
439 Pacific). *Mar. Geophys. Res.* 17/1, 17-35.
- 440
- 441 Ennadifi, M.Y., 1975. Carte Géologique du Maroc au 1/100000, 1975, Service Géologie du Maroc, Rabat.
- 442
- 443 Essahlaoui, A., Sahbi, H., El-Yamine, N., 2002. Application de la géophysique (method géoélectrique) à la
444 reconnaissance du plateau de Meknès. *Geologica Belgica*, 2000, 35-53
- 445
- 446 Essahlaoui, A., El Ouali, A., 2003. Détermination de la structure géologique de la partie Sud de la plaine du
447 Saïss (bassin de Meknes-Fes, Maroc) par la méthode géoélectrique. *Bulletin of Engineering Geology and*
448 *the Environment*, 62, 155-166,
- 449
- 450 Essahlaoui, A., Sahbi, H., e, B.L., El-Yamine, N., 2001. Reconnaissance de la structure géologique du bassin de
451 Saïss occidental, Maroc, par sondages électriques. *Journal of African Earth Sciences*. 32 , 777-789.
- 452
- 453 Fassi, D., 1999. Les formations superficielles du Saïss de Fès et de Méknès. *Notes et mémoires du service*
454 *géologique*. 389, pp. 527
- 455
- 456 Frizon de Lamotte, D., Leturmy, P., Missenard, Y., Khomsi, S., Ruiz, G., Saddiqi, O., Guillocheau, F., Michard,
457 A., 2009. Mesozoic and Cenozoic vertical movements in the Atlas system (Algeria, Morocco, Tunisia): An
458 overview. *Tectonophysics*. 475, 9-28.
- 459
- 460 Harmouzi, O., 2010. Reconnaissance détaillée de la partie nord-est du Bassin de Saïss (MAROC): interprétation
461 de sondages électriques verticaux par combinaison des méthodes statistique, géostatistique et d'inversion,
462 UFR: *Geologie de surface et environnement*. university of Moulay Ismail. pp. 323.
- 463
- 464 Jabour, N., Kasmi, M., Menzhi, M., Birouk, A., Hni, L., Hahou, Y., Timoulali, Y., Badrane, S., 2004. The
465 February 24 2004 Al Hoceima earthquake. *European-Mediterranean Seismic Centre Newsletter*. 21, 7-10.
- 466

- 467 Perrin, J.L., Raïs, N., Chahinian, N., Moulin, P., Ijjaali, M. 2014. Water quality assessment of highly polluted
468 rivers in a semi-arid Mediterranean zone Oued Fez and Sebou River (Morocco), *Journal of Hydrology*, 510,
469 26-34,
470
- 471 Piqué, A., Tricart, P., Guiraud, R., Laville, E., Bouaziz, S., Amrhar, M., Aït Ouali, R., 2002. The Mesozoic–
472 Cenozoic Atlas belt (North Africa): an overview. *Geodinamica Acta*. 15, 85–208.
473
- 474 Qarqori, K., Rouai, M., Moreau, F., Saracco, G., Dauteuil, Hermitte, D., Boualoul, M., Le Carlier de Veslud, C.,
475 2012. Geo-electrical tomography investigating and modeling of fractures network around Bittit spring
476 (Middle Atlas, Morocco). *International Journal of Geophysics*. Pp. 13
477
- 478 Vergés, J., Manel Fernández, M. 2012. Tethys–Atlantic interaction along the Iberia–Africa plate boundary: The
479 Betic–Rif orogenic system *Tectonophysics* 579, 144–172
480
- 481 Wood, J. (2013) LandSerf 2.3, <http://www.landserf.org>
482
- 483 Zarhloule, Y., Lahrache, A., Ben Abidate, L., Khattach, D., Bour, S., Boukdir, A., Ben Dhia, H., 2001. La
484 prospection géothermique de surface au Maroc: hydrodynamisme, anomalies thermiques et indices de
485 surface. *Journal of African Earth Sciences*. 32, 851-867.
- 486 Zizi M. (2002) Triassic-Jurassic extensional systems and their Neogene reactivation in northern morocco: the
487 rides Prerifaines and Guercif basin. *Notes et mémoires du service géologique marocain*, 416.

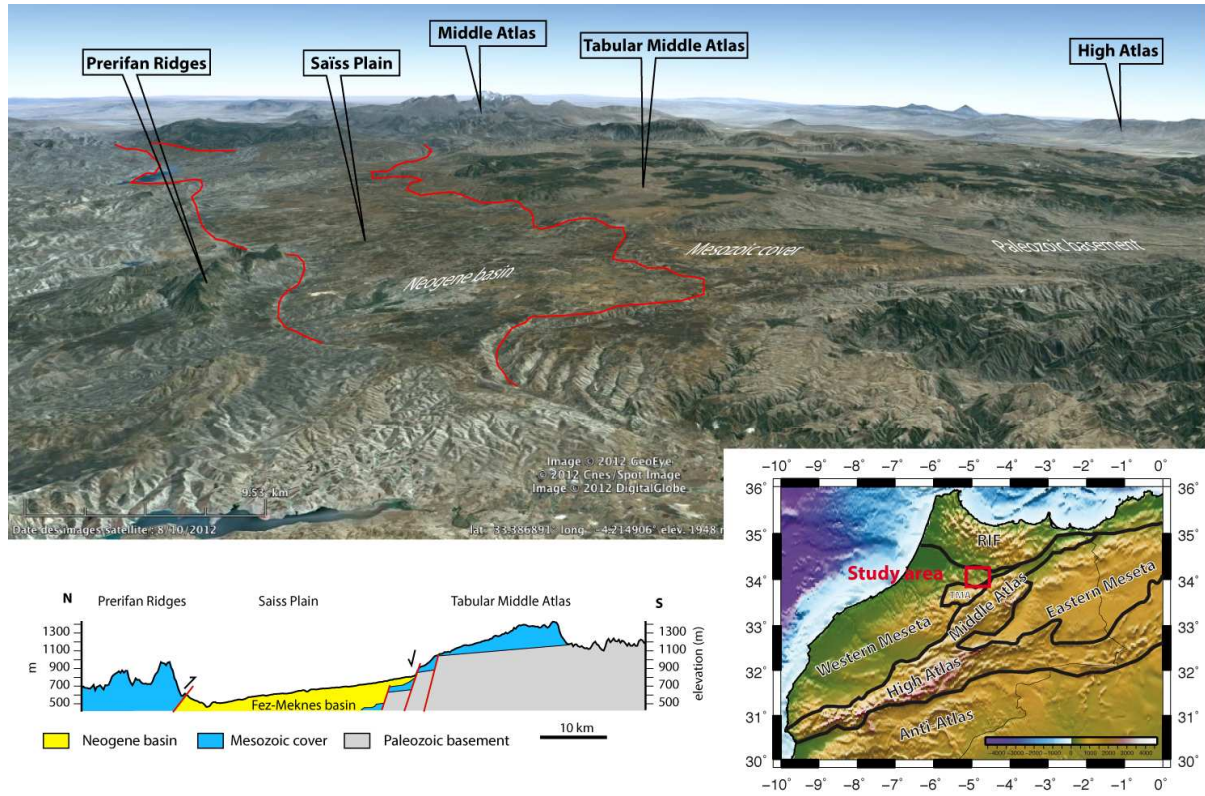


Figure 1

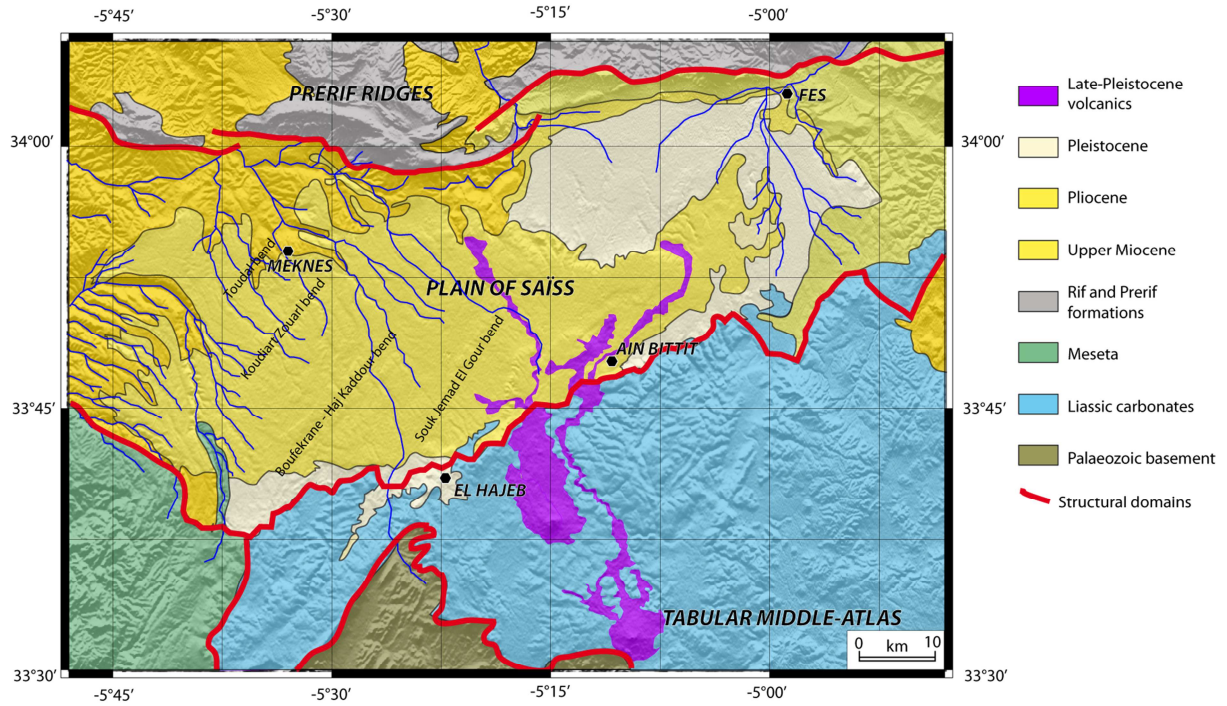


Figure 2

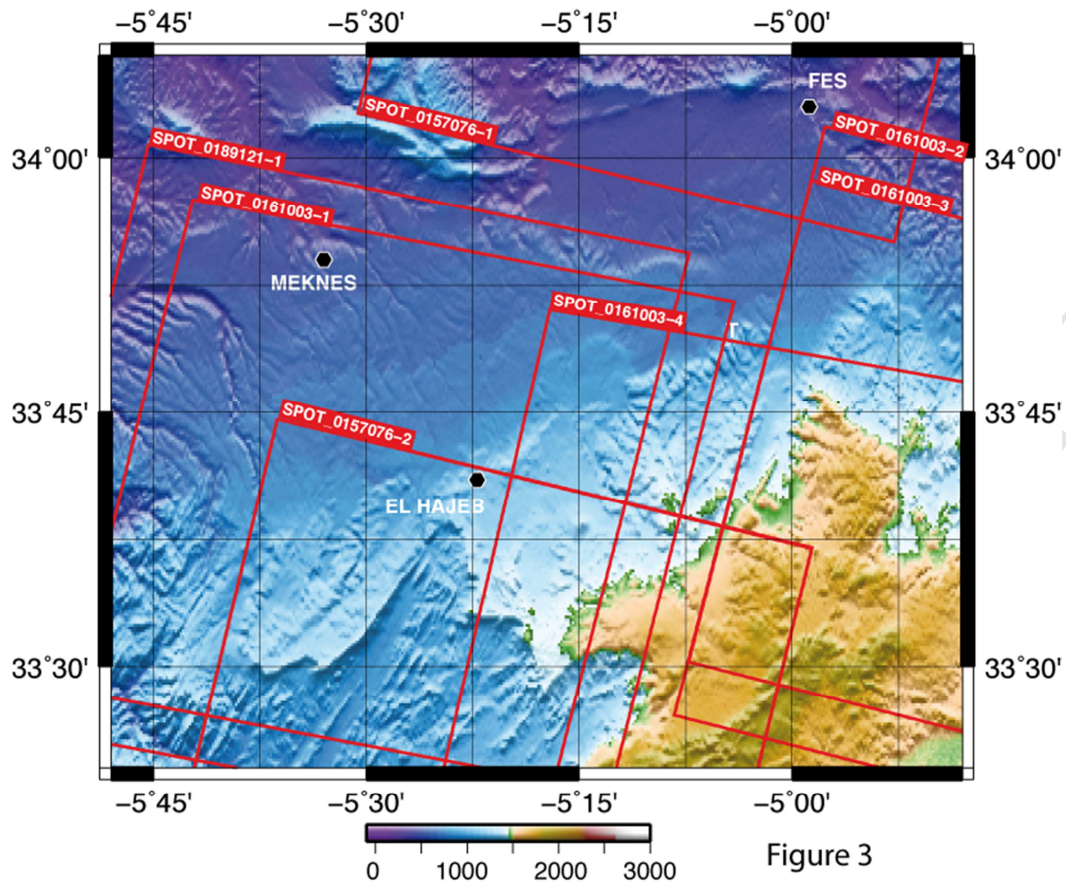
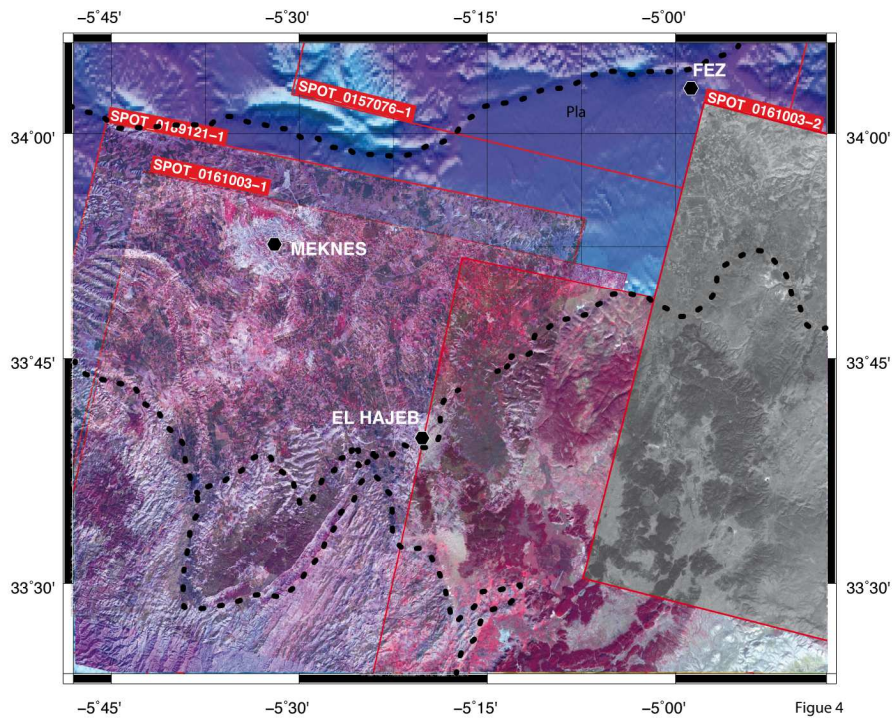
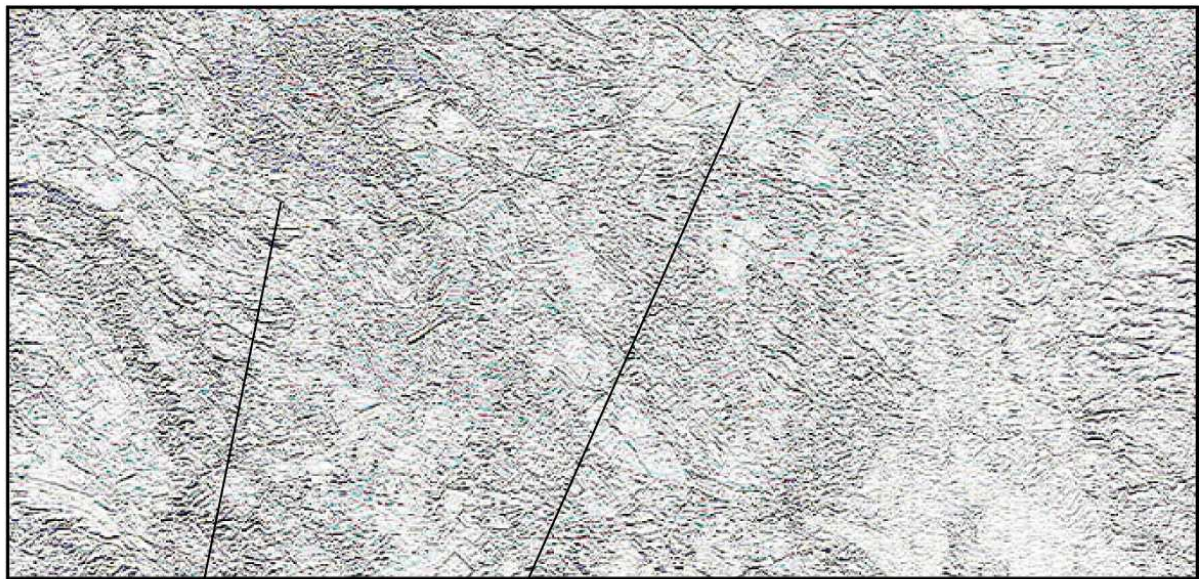


Figure 3



ACCEPTED MANUSCRIPT

N-S convolution matrix (5x5 pixels)



NW-SE convolution matrix (5x5 pixels)

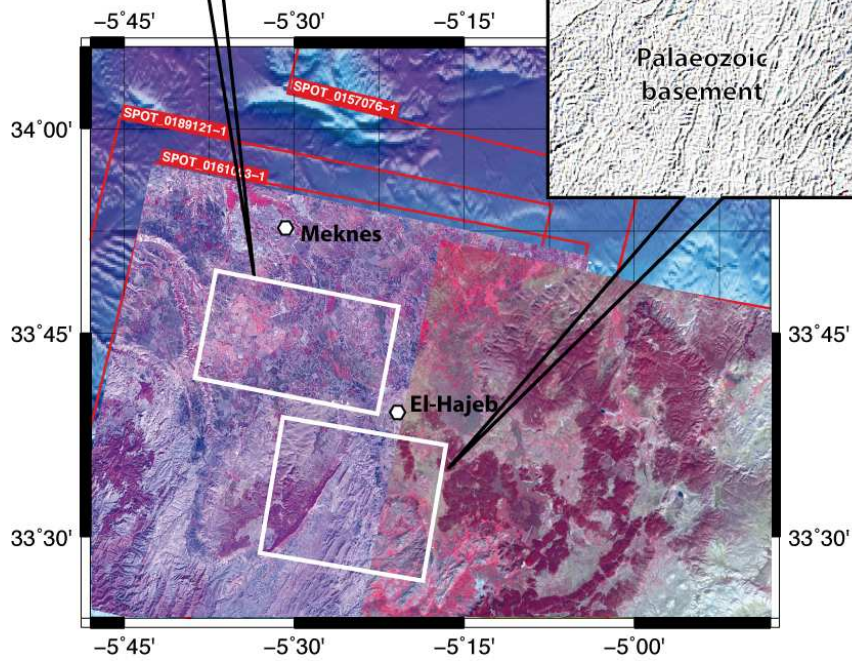
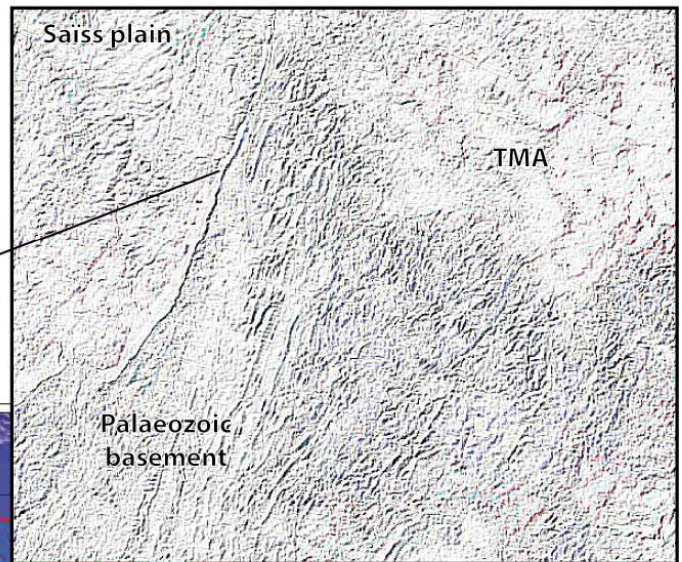


Figure 5

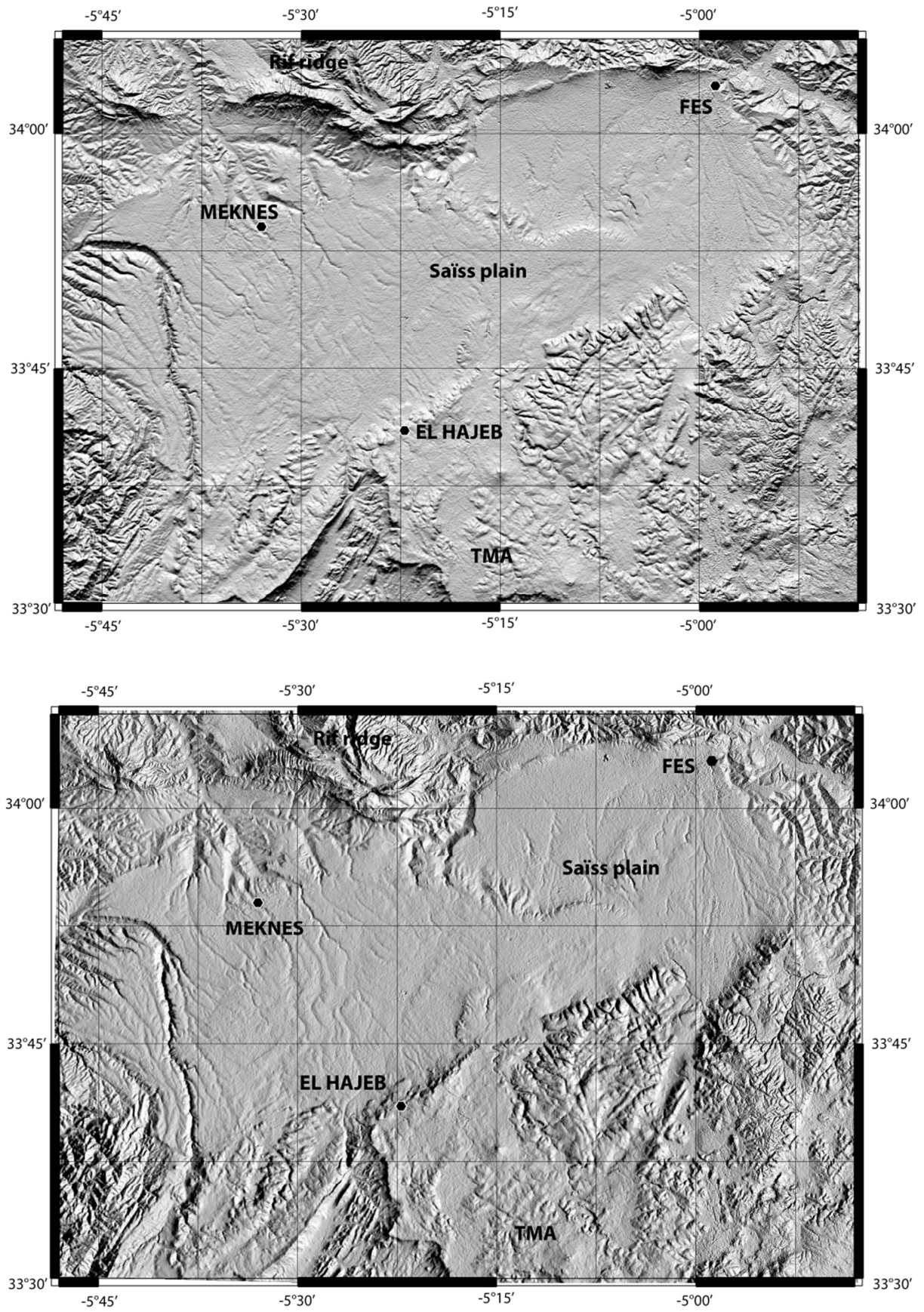
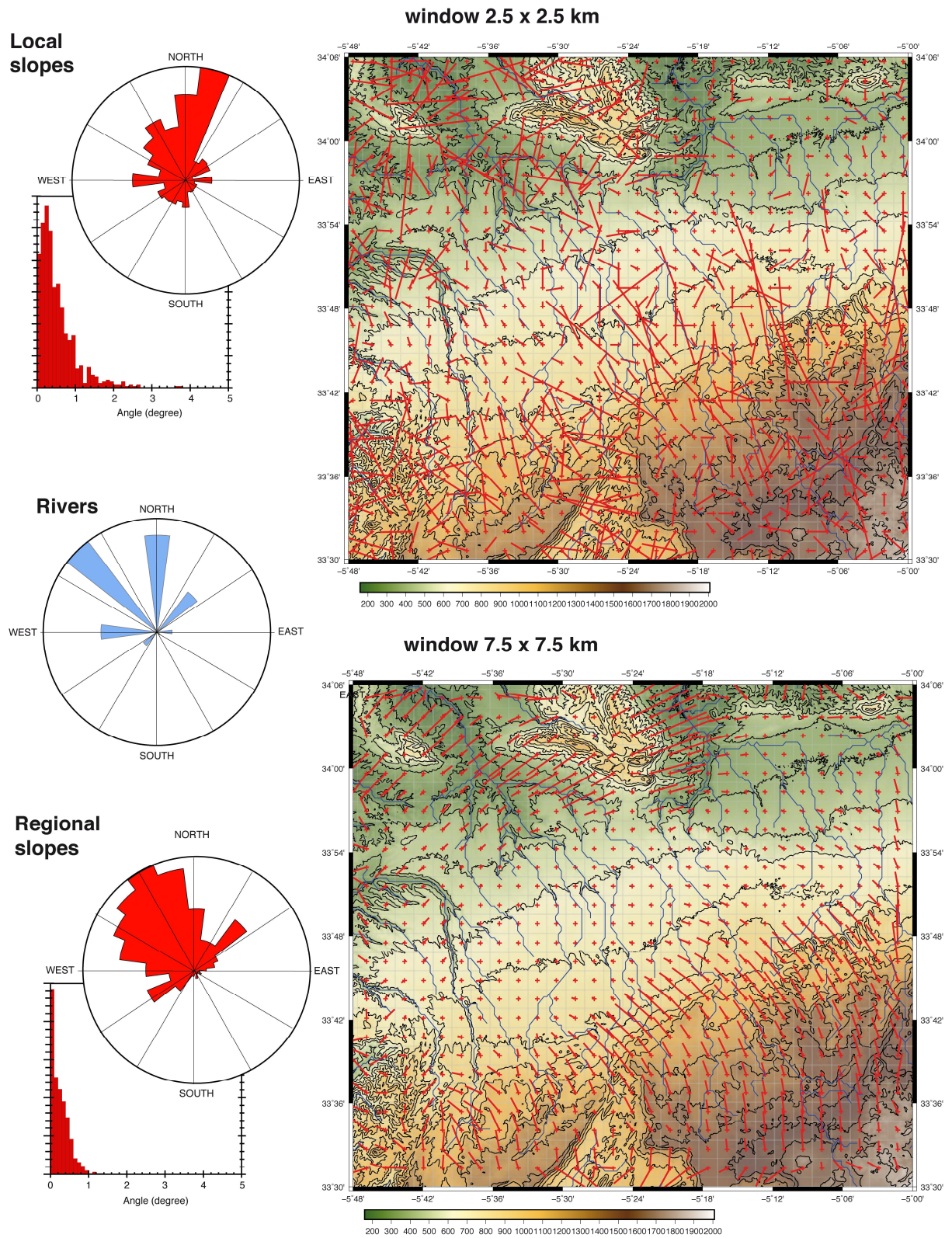


Figure 6



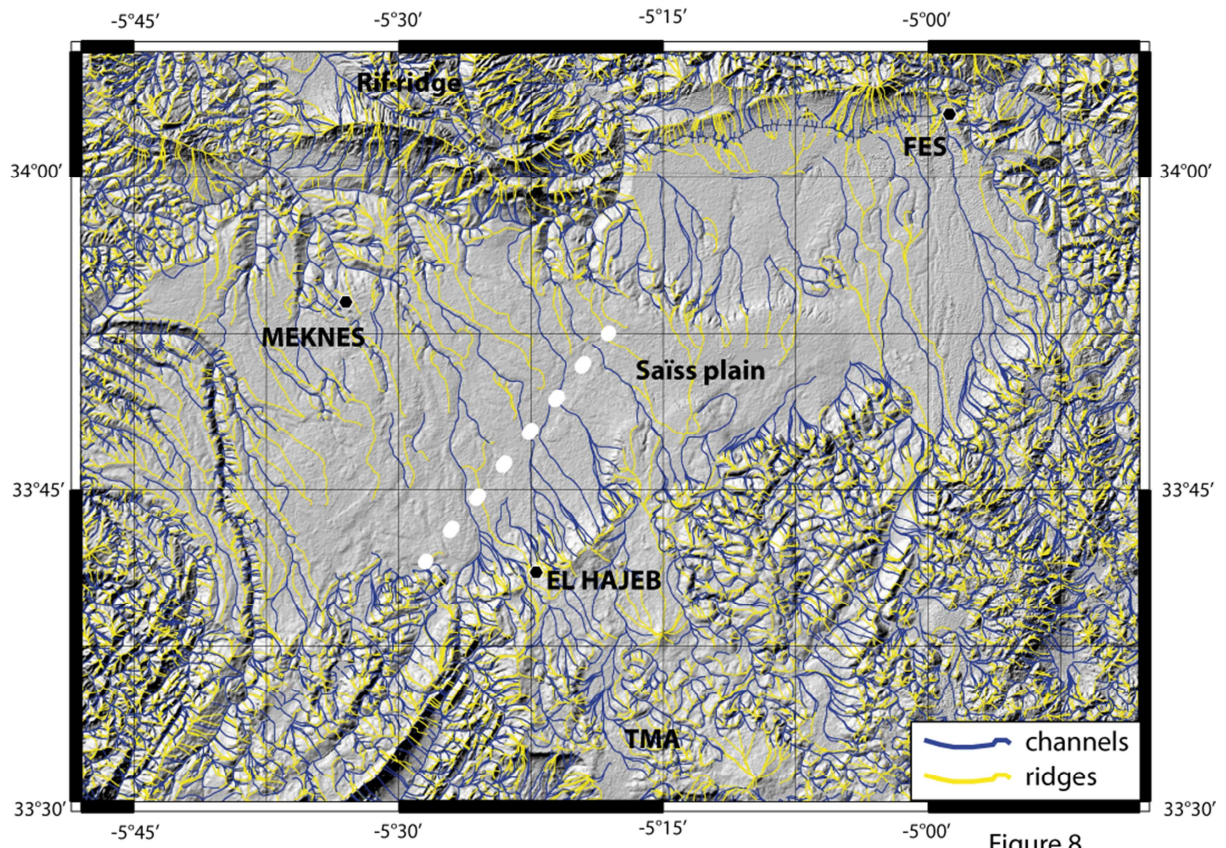


Figure 8

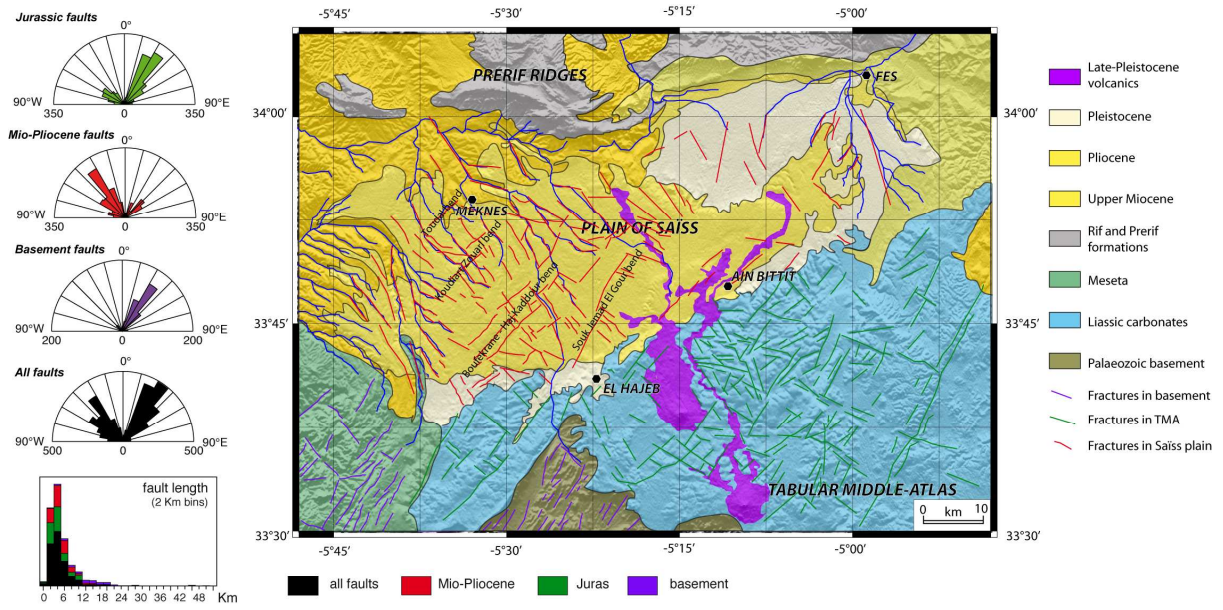


Figure 9

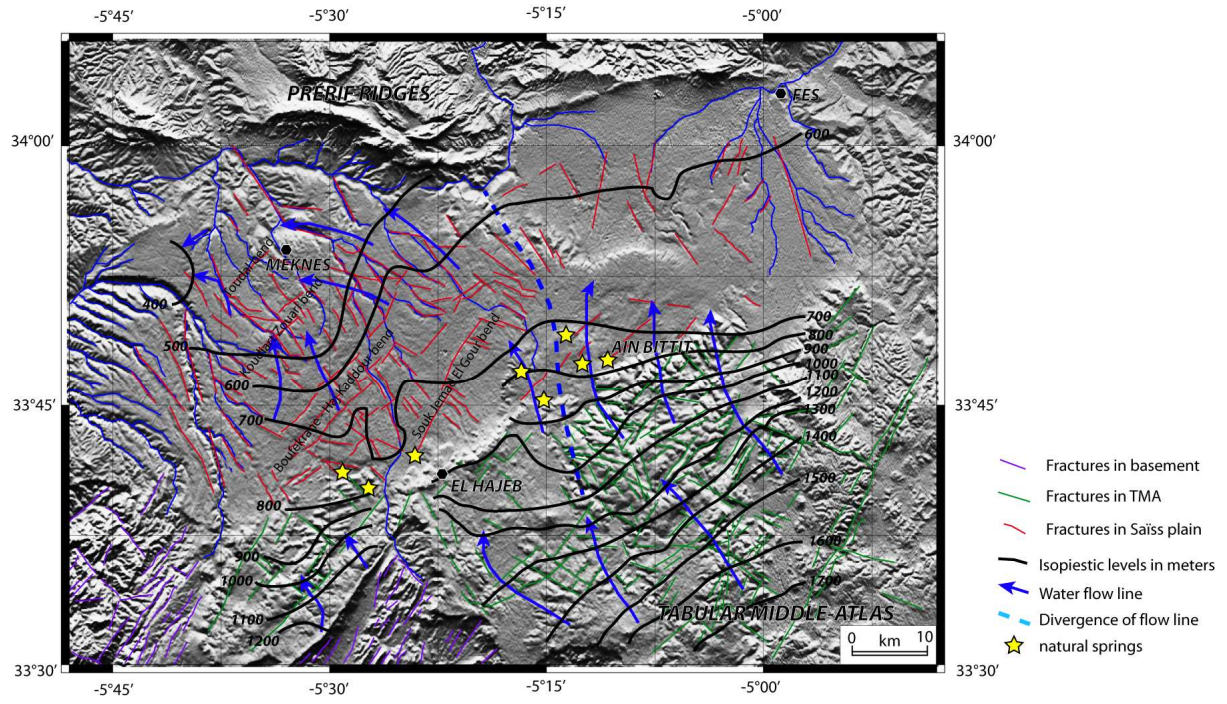


Figure 10

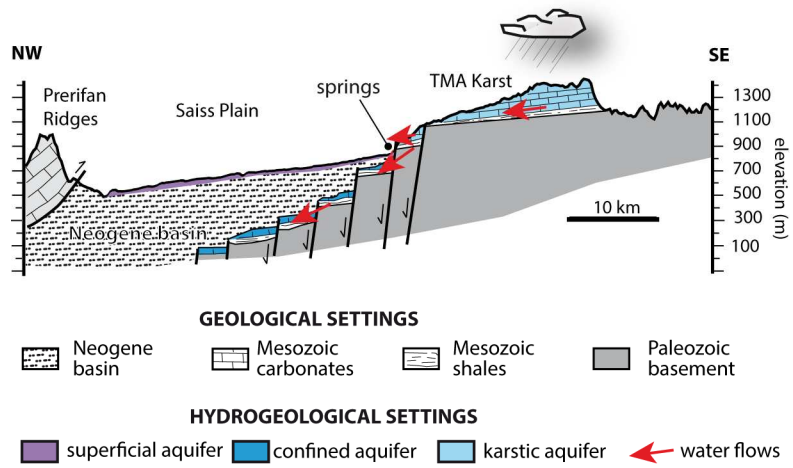


figure 11

Research Highlights:

- We mapped fracture pattern in Saïss basin and Middle-Atlas with SPOT images and DEM.
- We pointed out a new fracture set trending NW-SE in addition to famous NE-SW trend.
- The NE fractures control the water paths from the Middle-Atlas to the Saïss basin.
- We propose a model of water circulation from the TMA to the Saïss basin.